TÜBİTAK

Turkish Journal of Earth Sciences

http://journals.tubitak.gov.tr/earth/

Research Article

Turkish J Earth Sci
(2018) 27: 249-268

doi:10.3906/yer-1711-3

Geochemistry and source characteristics of Dehsard mafic volcanic rocks in the southeast of the Sanandaj–Sirjan zone, Iran: implications for the evolution of the Neo-Tethys Ocean

Mohammadali NAZEMEI, Mohsen ARVIN*, Sara DARGAHI
Department of Geology, Faculty of Sciences, Shahid Bahonar University of Kerman, Kerman, Iran

Received: 04.11.2017 • **Accepted/Published Online:** 13.05.2018 • **Final Version:** 24.07.2018

Abstract: The Late Jurassic–Early Cretaceous Dehsard mafic volcanic rocks crop out in the southeastern Sanandaj–Sirjan Zone (SSZ), composed primarily of basalts and basaltic andesite with subordinate dolerite. They are influenced to some degree by hydrothermal alteration under zeolite–greenschist facies. Using fairly immobile trace elements, the mafic volcanic rocks show subalkaline (tholeiitic) affinities. They commonly have similar designs with somewhat strong enrichment in light rare earth elements (LREEs) and large ion lithophile elements (LILEs) and depletion in high field strength elements (HFSEs; e.g., Nb, Ta, Ti) and nearly flat heavy rare earth element (HREE) patterns. The negligible or absence of negative Eu anomalies indicate that plagioclase played an insignificant role during magma evolution. The low La/Nb (1.03–2.31) and Nb/Y (0.12–0.46) ratios, relatively high Zr/Y (4.03–8.18) and Th/Ta (2.25–9.64) ratios, steady enhanced normalized patterns, and moderate La/Nb ratios hint at an island arc and most likely a back-arc basin environment for the formation of Dehsard mafic volcanic rocks. The arc magma resulted from partial melting of depleted mantle source that experienced assimilation and fractional crystallization and was enhanced by melts of subducted sediments or contribution of slab-derived fluids in an intraoceanic subduction environment in the Neo-Tethyan Ocean. Therefore, the presence of an island arc setting (Dehsard island arc) must be investigated in the south of the SSZ prior to the Late Jurassic–Early Cretaceous as the Neo-Tethys oceanic crust was subducting north beneath the southern margin of the Central Iranian Microcontinents. The later collision of the arc with SSZ led to tectonic proximity of the Dehsard mafic volcanic rocks to SSZ components.

Key words: Volcanic rocks, subduction, Sanandaj–Sirjan zone, back-arc basin, Neo-Tethys, petrogenesis

1. Introduction

The Zagros Orogenic Belt (ZOB) of Iran belongs to the Alpine–Himalayan orogenic belt that was formed as a result of collision between the Arabian and Eurasian plates during Cenozoic times, separating the Arabian platform from the large plateaus of Central Iran (Stocklin, 1968; Förster et al., 1972; Jung et al., 1976; Berberian et al., 1982; McKenzie and O'Nions, 1991; Ahmad and Posht Kuhi, 1993; Shaker Ardakani, 2016). The ZOB and the Iranian plateau preserve a long record of convergence history (since 150 Ma) between Eurasia and Arabia across the Neo-Tethys Ocean, from subduction and obduction development to present-day collision (Ahmad and Posht Kuhi, 1993). The ZOB structurally consists of three parallel NW–SE trending tectonic units: (1) the UDMA, (2) the Sanandaj–Sirjan Zone (SSZ), and (3) the Zagros Folded-Thrust Belt (ZFTB) (Alavi, 2004) (Figure 1a). The UDMA or Urumieh–Dokhtar volcanic zone of Schroeder (1944) is an approximately 150-km wide magmatic association and has been explained to be an active subduction related Andean type magmatic arc since the Late Jurassic to present (Berberian and King, 1981; Berberian et al., 1982). It is composed of extensive tholeiitic, calc-alkaline, and K-rich alkaline intrusive and extrusive rocks (accompanied with pyroclastic and volcanoclastic sequences) alongside the active margin of the Iranian plates. The calc-alkaline intrusive rocks (cutting Upper Jurassic formations and overlain unconformably by Lower Cretaceous fossiliferous limestone) and the alkaline and calc-alkaline lava flows and pyroclastic rocks of Pliocene to Quaternary volcanic cones are respectively the oldest and youngest rocks in the UDMA (Berberian and King, 1981). The ZFTB comprises a thick and nearly continuous sequence of Paleozoic to Late Tertiary shelf sediments that were separated from the Precambrian metamorphic basement by 1–2 km of thick Infra-Cambrian Hormoz salt formation (Alavi, 2004; Agard et al., 2005). The metamorphic belt of the SSZ consists mainly of various metamorphic, igneous, and

* Correspondence: arvin@uk.ac.ir

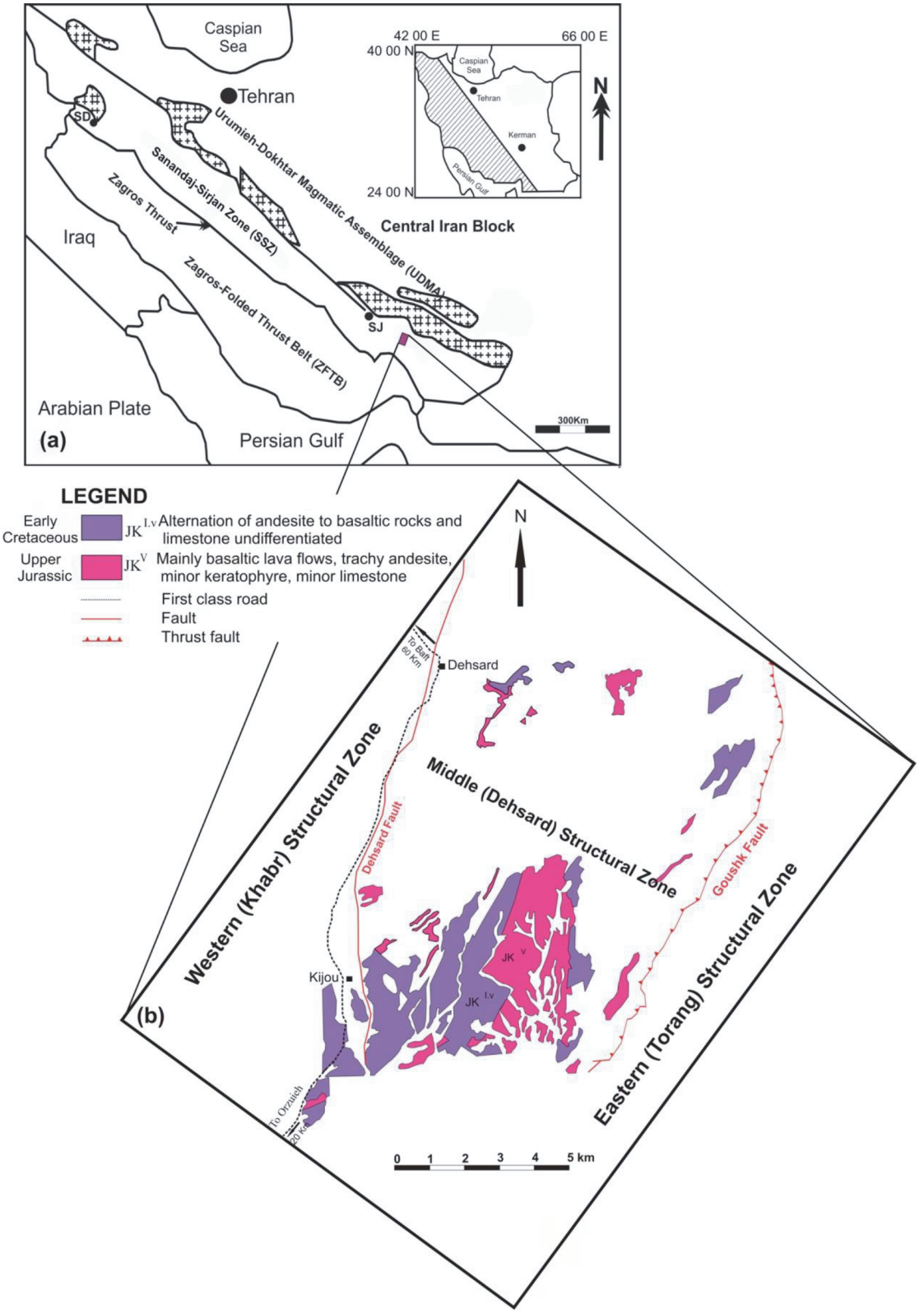

Figure 1. Simplified geological map of Iran showing three tectonic subdivisions of Zagros orogenic belt and study area (after Sedighian et al., 2017); S.J = Sirjan; (b) Simplified geological/structural map of the Dehsard (Bazar) (modified from Geological map of the Dehsard (Bezar), Scale 1/100,000, Nazemzadeh and Rashidi, 2006).

sedimentary rocks of Late Neoproterozoic to Neogene age that are unconformably overlain by the Barremo–Aptian Orbitolina limestones, characteristic of Central Iran sedimentation (Berberian and Berberian, 1981; Berberian et al., 1982; Temizel and Arslan, 2008; Shahbazi et al., 2010; Fergusson et al., 2016). The SSZ was deformed and partly unearthed during the Cretaceous–Paleogene continental collision of the Afro-Arabian with Central Iran (Şengör and Natal'in, 1996; Mohajjel and Fergusson, 2000; Mohajjel et al., 2003). For most of the second half of the Mesozoic, the SSZ manifested an active Andean-type margin where its calc-alkaline magmatic activity constantly moved northward (Berberian and King, 1981). The SSZ and its metamorphic–plutonic complexes were the subject of numerous petrological, geochemical, structural, and geochronological studies (Baharifar et al., 2004; Ahmadi Khalaji et al., 2007; Arvin et al., 2007; Shahbazi et al., 2010; Esna-Ashari et al., 2012, Fergusson et al., 2016; Amiri et al., 2017; Sedighian et al., 2017). The aim of the present contribution is to present detail petrographic and whole-rock geochemical analysis of mafic volcanic rocks in the SSZ, which are exposed in the south of the Dehsard area southwest of Kerman (Figure 1b), in order to examine their origin and tectonic settings in the context of the Neo-Tethys evolution.

2. Sampling and analytical techniques

A total of 240 samples were collected from mafic volcanic rocks. After detailed petrographic studies of thin sections, 26 samples with the least alteration side effect were chosen and finely powdered in an agate mill for whole-rock geochemical analysis. The whole rock analyses were conducted at the ALS Chemex Geochemistry Laboratories in Vancouver, Canada. First 0.200 g of ground sample was mixed well with 0.9 g of lithium metaborate flux and fused in a furnace at 1000 °C. The resulting melt was cooled and then dissolved in 100 mL of 4% HNO_3/2% HCl solution. This solution was then analyzed by inductive coupled plasma-atomic emission spectroscopy (ICP-AES, for major elements using geochemical procedure ME-ICP06) and inductive coupled plasma-mass spectrometry (ICP-MS, for trace and rare earth elements using geochemical procedure ME-MS81). Oxide concentration was calculated from the determined elemental concentration and the result is reported in that format. Quality control limits for reference materials and duplicate analyses were established according to the precision and accuracy requirements of the particular methods. The results of analyses together with detection limits for each element are presented in the Table. Furthermore, for measuring the loss on ignition (LOI) 1.0 g of prepared sample was placed for 1 h in an oven at 1000 °C, then cooled, and weighed. The LOI was calculated by weight difference.

3. Geology and field relationships

The Dehsard area is located 260 km southwest of Kerman, in the southernmost part of the SSZ (Figure 1a), and is outlined on the Dehsard (Bazar) geological map (Nazemzadeh and Rashidi, 2006). The map is divided into three structural zones: Western (Khabr), Middle (Dehsard), and Eastern (Torang), separated by two north–south running faults of Dehsard and Goushk (Figure 1b). Under the influence of these two faults the trend of the SSZ in the study area has changed from NW–SE to N–S. They also triggered some shattering in volcanic rocks and changed their trends from east–west to north–south (Sabzehei, 1994). The Late Jurassic–Early Cretaceous Dehsard mafic volcanic rocks lie in the Middle (Dehsard) structural zone and are outcropped in the JK^{LV} unit (consists of alternation of andesite to basaltic rocks and limestone undifferentiated) and JK^{V} subunit (consists mainly of basaltic lava flows, trachyandesite, minor keratophyre, and minor limestone) (Figure 1b) (Nazemzadeh and Rashidi, 2006).

The mafic volcanic rocks appear as grayish black to light brown and mainly consist of basalt and basaltic andesite lava flows with subordinate dolerite. The lava flows, occasionally with microphenocrysts of plagioclase and pyroxene (up to 2 mm in size) in aphyric groundmass, are exposed as both nonvesicular/vesicular massive rocks and their thickness varies between 2 and 70 m. The vesicles, 1 to 5 mm in diameter, are rounded to oval and filled often with secondary minerals, such as calcite, chlorite, epidote, and quartz. Frequently it is possible to separate different lava flows. They are influenced by various degrees of subseafloor hydrothermal alteration. The sedimentary rocks mainly occur as layered to massive micritic limestones with minor shaley/marly limestones. Their thickness varies between 1 and 8 m and they occur as intercalated layers with mafic volcanic rocks (Figure 2). They are for the most part in tectonic contact with mafic rocks.

4. Petrography

Mineralogically the Dehsard basalts and basaltic andesites are composed primarily of plagioclase and clinopyroxene phenocrysts, set in an aphanitic matrix of the same minerals associated with opaque and apatite as accessory phases. They display subaphyric, porphyritic, glomeroporphyritic, interstitial, pilotaxitic, variolitic, and amygdaloidal textures (Figures 3a and 3b). Dolerite is mineralogically the same as basalt and basaltic-andesite but show subophitic texture (Figure 3c). The vesicles are filled with secondary minerals such as calcite, chlorite, and quartz along with elongated radial shape epidote and zeolites, which were formed during submarine hydrothermal alteration (Thompson, 1991). Other secondary minerals are actinolite, titanite, and prehnite. The plagioclases for

Table. Whole rock geochemical data of representative samples of Dehsard mafic volcanic rocks. Major elements in wt.%, trace elements in ppm. Total iron as Fe_2O_3; LOI = Loss on ignition; D.L.= Detection limit; Mg# = (MgO/(FeO + MgO)) [mol.%].

		Basalt							
Sample	D.L.	NC10	NC15	NC16	ND5	NE10	NF14	NF19	NF29
Latitude (°N)	-	28.2856	28.2870	28.2870	28.2895	28.2908	28.3001	28.3007	28.3010
Longitude (°E)	-	56.2935	56.2940	56.2940	56.2979	56.3027	56.3124	56.3112	56.3123
SiO_2	0.01	49.3	47	50.6	50.3	51.4	50.6	48.8	46.7
Al_2O_3	0.01	19.1	18.2	15.65	16.25	15.6	15.7	17.05	16.05
TiO_2	0.01	1.11	1.24	1.6	1.3	1.77	2.23	1.09	1.21
Fe_2O_3	0.01	8.06	8.82	10	8.76	10.1	11.6	8.59	8.78
CaO	0.01	10.9	10.75	7.75	8.11	7.16	8.62	8.53	8.39
MgO	0.01	5.48	5.79	5.06	5.53	4.53	5.53	8.29	9.77
MnO	0.01	0.12	0.15	0.21	0.13	0.23	0.21	0.21	0.15
Na_2O	0.01	2.67	3.19	3.66	3.64	3.43	3.95	3.46	2.62
K_2O	0.01	1.27	0.91	1.13	0.76	1.46	0.65	0.4	0.54
P_2O_5	0.01	0.16	0.22	0.29	0.26	0.45	0.53	0.16	0.22
Cr_2O_3	0.01	0.02	0.02	0.01	0.02	0.01	0.02	0.03	0.06
SrO	0.01	0.06	0.04	0.05	0.06	0.05	0.05	0.04	0.03
BaO	0.01	0.02	0.02	0.03	0.02	0.04	0.02	0.02	0.02
LOI	0.01	2.35	2.74	2.11	3.07	3	1.94	3.66	4.08
Total	-	100.62	99.09	98.15	98.21	99.23	101.65	100.33	98.62
Ba	0.5	167	154.5	267	164.5	371	234	164.5	148
Cr	10	150	170	80	140	60	120	220	440
Cs	0.01	1.58	0.49	0.51	0.43	0.36	0.41	1.06	0.91
Nb	0.2	4.3	6.4	13.6	10.1	13.3	11.5	2.6	4.9
Rb	0.2	36.5	16	10.8	8.5	29.1	12.3	7.9	12.6
Sr	0.1	548	418	445	541	446	448	421	307
Th	0.05	1.19	1.4	4.36	3.12	3.67	3.53	0.62	0.95
V	5	198	216	231	199	222	323	213	194
Y	0.5	19.6	24.3	35.5	28.7	34.6	37.1	22.1	23
Zr	2	100	129	208	206	216	179	94	121
Ni	1	54	72	66	53	49	87	127	265
Hf	0.2	2.3	3	4.9	4.7	4.6	4.1	2.2	2.6
Ga	0.1	18.7	19.2	22.2	19.5	20.6	22.7	17.9	17.6
Sn	1	1	1	2	2	2	2	1	1
Ta	0.1	0.3	0.5	0.9	0.6	0.8	0.7	0.2	0.3
Tm	0.01	0.31	0.39	0.59	0.45	0.55	0.56	0.31	0.36
U	0.05	0.2	0.4	1.31	0.55	0.84	0.89	0.1	0.32
W	1	1	16	10	1	1	2	3	1
La	0.5	8.6	10.5	20.9	15.6	25.6	24.3	6	9.3
Ce	0.5	20.5	24.3	44.8	35.1	53.9	50.8	15.9	22.5
Pr	0.03	2.75	3.25	5.53	4.46	6.6	6.4	2.37	3.08
Nd	0.1	12.2	14.4	23.6	19.5	26.7	28.4	11.1	13.8

Table. (Continued).

Sm	0.03	3.08	3.62	5.6	4.58	6.42	6.37	3.22	3.28
Eu	0.03	1.13	1.32	1.73	1.46	1.95	2.32	1.12	1.24
Gd	0.05	3.58	4.41	6.25	5.04	6.6	7.31	3.64	3.94
Tb	0.01	0.6	0.67	1.05	0.84	1.05	1.12	0.64	0.68
Dy	0.05	3.73	4.38	6.62	5	6.28	6.65	3.68	4.25
Ho	0.01	0.76	0.95	1.41	1.08	1.33	1.45	0.82	0.9
Er	0.03	2.15	2.79	3.97	3.16	3.66	4.25	2.32	2.55
Yb	0.03	2.04	2.6	3.62	3.08	3.35	3.56	2.21	2.24
Lu	0.01	0.31	0.42	0.59	0.44	0.57	0.51	0.34	0.34
Mg#		0.55	0.54	0.47	0.53	0.44	0.46	0.63	0.66
Rb/Sr		0.067	0.038	0.024	0.016	0.065	0.027	0.019	0.041
Sm/Nd		0.252	0.251	0.237	0.235	0.240	0.224	0.290	0.238

Table. (Continued).

	Basalt								
Sample	NG2	NG19	NG22	NG44	NG45	NJ1	NM2-1	NO12	NP12
Latitude (°N)	28.3036	28.3074	28.3074	28.3130	28.3130	28.2920	28.2571	28.2599	28.2991
Longitude (°E)	56.3078	56.3133	56.3133	56.3144	56.3144	56.2938	56.2281	56.2462	56.3044
SiO_2	49.6	48.2	48.1	47.7	48.8	47.6	47.5	50.9	49.3
Al_2O_3	19.65	15.5	17.5	16.65	17.15	17.75	14.25	13.6	14.6
TiO_2	1.48	1.4	1.26	1.39	1.94	1.11	2.27	2.45	2.53
Fe_2O_3	8.97	11.1	9.24	9.94	10.9	8.22	13.4	13.3	13.15
CaO	9.66	9.96	9.72	8.76	6.9	8.7	8.05	4.95	10.2
MgO	5.45	7.09	6.3	7.08	4.99	8.97	5.49	3.63	5.2
MnO	0.16	0.17	0.17	0.14	0.14	0.14	0.25	0.15	0.28
Na_2O	3.62	3.06	2.71	2.93	4.07	3.15	3.67	5.79	3.38
K_2O	0.75	0.4	1.07	1.13	1.47	0.5	0.8	0.07	0.89
P_2O_5	0.23	0.18	0.2	0.23	0.32	0.12	0.31	0.48	0.44
Cr_2O_3	0.02	0.03	0.02	0.03	0.01	0.03	0.01	<0.01	0.01
SrO	0.06	0.03	0.03	0.06	0.06	0.04	0.04	0.02	0.06
BaO	0.02	0.01	0.03	0.05	0.04	0.01	0.02	0.01	0.02
LOI	2.29	2.75	3.24	4.38	2.4	4.07	2.6	3.81	1.68
Total	101.96	99.88	99.59	100.47	99.19	100.41	98.66	99.16	101.74
Ba	206	81.2	245	452	377	63.7	146.5	49.6	222
Cr	130	200	170	190	70	200	70	20	90
Cs	0.82	0.56	0.66	0.36	1.67	4.02	1.59	0.15	0.79
Nb	9.1	4.6	6.4	7.5	11.3	3.7	7.8	9.7	12
Rb	10.9	9.4	21	13.1	22.9	10.7	17.7	0.6	20.7
Sr	484	318	325	507	533	381	344	150.5	483
Th	1.81	0.95	1.46	1.01	2.28	1.39	1.88	2.15	1.59
V	239	267	215	238	275	183	324	305	336

Table. (Continued).

Y	22.8	28.8	24.2	22.9	29.3	18.6	40.4	41.6	36.8
Zr	134	117	130	114	180	87	198	206	196
Ni	40	60	71	86	26	147	39	9	26
Hf	2.9	2.8	2.8	2.5	3.8	2.3	4.5	4.7	4.4
Ga	21.1	19.9	18.4	18.9	22.5	16	21.4	21.5	21.1
Sn	1	1	1	1	2	1	2	1	2
Ta	0.5	0.3	0.4	0.4	0.7	0.2	0.5	0.6	0.6
Tm	0.34	0.5	0.42	0.37	0.51	0.33	0.62	0.66	0.57
U	0.5	0.22	0.49	0.24	0.54	0.12	0.52	0.59	0.54
W	4	2	1	2	2	2	1	<1	2
La	14	8.7	9	10.9	16.9	6.3	12.8	18.5	16.7
Ce	29.6	21.3	20.9	24.5	37	15.6	32.1	43.5	38.8
Pr	3.62	2.98	2.8	3.25	4.85	2.27	4.49	5.85	5.3
Nd	16.1	14.1	12.8	14.4	20.4	10.3	21.3	26.7	23.7
Sm	3.75	3.73	3.28	3.49	5.07	2.78	5.87	7.15	6.13
Eu	1.4	1.54	1.18	1.39	1.84	0.99	2	2.5	2.19
Gd	4.14	4.51	4.12	4.11	5.43	3.37	6.91	7.63	6.94
Tb	0.69	0.83	0.66	0.67	0.94	0.58	1.12	1.28	1.11
Dy	4.24	5.06	4.4	4.23	5.56	3.48	7.1	7.74	6.84
Ho	0.87	1.07	0.93	0.88	1.1	0.74	1.54	1.59	1.41
Er	2.44	3.01	2.66	2.56	3.13	2.08	4.58	4.66	3.89
Yb	2.21	3.09	2.6	2.24	3.09	1.96	4.25	4.15	3.43
Lu	0.35	0.44	0.37	0.35	0.44	0.31	0.62	0.65	0.53
Mg#	0.52	0.53	0.55	0.56	0.45	0.66	0.42	0.33	0.41
Rb/Sr	0.023	0.030	0.065	0.026	0.043	0.028	0.051	0.004	0.043
Sm/Nd	0.233	0.265	0.256	0.242	0.249	0.270	0.276	0.268	0.259

Table. (Continued).

	Basalt	Basaltic andesite						Dolerite	
Sample	NP16	NA7	NB4	NB22	NB28	NF13	NO1	NM	NM2
Latitude (°N)	28.2981	28.3526	28.3964	28.4055	28.2832	28.3001	28.2796	28.2615	28.2578
Longitude (°E)	56.3022	56.3758	56.3867	*56.4022*	56.2891	56.3124	56.2806	56.2330	56.2302
SiO_2	47.8	53	52.5	55.6	52.7	52.5	53.5	48.2	47.6
Al_2O_3	16.55	14.9	15.55	16.3	15.75	14.3	15.55	13.25	13.05
TiO_2	1.19	2.21	1.98	1.09	1.99	2.2	1.17	2.91	2.9
Fe_2O_3	9.69	10.05	10.45	7.49	11	9.84	6.5	16.15	15.75
CaO	10.9	5.99	6.89	6.7	7.93	5.54	4.81	8.51	8.36
MgO	8.36	1.08	4.06	4.41	4.37	5.31	5.25	4.68	4.58

Table. (Continued).

MnO	0.17	0.11	0.24	0.11	0.45	0.12	0.09	0.28	0.26
Na_2O	2.21	5.46	4.89	3.43	3.92	5.57	5.02	3.91	3.91
K_2O	0.76	3.35	1.38	2.82	0.27	0.2	0.92	0.65	0.93
P_2O_5	0.14	0.51	0.65	0.24	0.47	0.63	0.22	0.38	0.38
Cr_2O_3	0.04	<0.01	0.01	0.01	0.01	<0.01	0.01	<0.01	<0.01
SrO	0.04	0.01	0.05	0.05	0.04	0.02	0.03	0.04	0.05
BaO	0.01	0.03	0.04	0.04	0.01	0.01	0.01	0.01	0.01
LOI	2.53	4.36	2.13	1.65	2.29	4.42	6.82	2.19	1.92
Total	100.39	101.06	100.82	99.94	101.2	100.66	99.9	101.16	99.7
Ba	75.5	268	378	396	130.5	49.4	79.6	101	110.5
Cr	280	<10	40	90	70	10	90	30	30
Cs	1.36	0.12	0.13	0.51	0.36	0.15	0.24	0.41	1.12
Nb	3.4	17.8	18.4	14.4	10.8	18.2	10.4	10	10
Rb	15.6	53	28.7	27.9	3.6	3.1	27.7	14.1	25.8
Sr	343	66.1	492	403	299	174.5	262	331	430
Th	0.45	5.61	5.04	7.21	3.52	4.1	6.75	2.47	2.24
V	209	161	241	148	255	268	176	406	404
Y	23.8	57.5	40.1	34.6	44.3	40	32.8	55.3	55.8
Zr	96	377	235	283	280	257	252	272	267
Ni	124	<5	34	65	45	15	36	30	29
Hf	2.4	8.2	5.4	6.6	6.2	5.6	5.8	6.3	6.1
Ga	16.9	22.4	22.7	19.3	22.2	20.6	20.6	24.2	24.1
Sn	1	3	1	3	2	2	2	3	3
Ta	0.2	1.1	0.9	0.9	0.6	1	0.7	0.7	0.6
Tm	0.37	0.89	0.62	0.62	0.72	0.62	0.51	0.92	0.87
U	0.14	1.21	1.24	2.06	0.88	1.13	2.06	0.71	0.71
W	2	4	2	1	1	3	2	4	5
La	5.1	18.3	32	23.6	21.1	34.4	19.8	16.5	16.3
Ce	13.9	48.9	65.1	50	48.2	65.9	43.9	41.2	41
Pr	2.04	7.11	7.81	6.05	6.31	7.57	5.42	5.91	5.75
Nd	10.3	32.7	32.3	24.1	29.1	30.7	22.3	28.1	27.4
Sm	3.28	9.04	7.45	5.75	7.01	6.61	4.98	7.96	7.81
Eu	1.15	2.74	2.43	1.39	2.1	2.16	1.51	2.58	2.6
Gd	3.71	9.75	7.49	5.71	7.81	7.36	5.37	9.38	9.19
Tb	0.64	1.64	1.19	0.99	1.35	1.16	0.95	1.54	1.57
Dy	4.25	10.3	7.77	6.06	7.89	7.33	5.85	10.35	9.94
Ho	0.91	2.28	1.59	1.29	1.7	1.48	1.24	2.13	2.14
Er	2.54	6.56	4.38	3.74	4.64	4.17	3.53	6.35	6.29
Yb	2.36	5.82	3.99	4.05	4.59	4.06	3.39	5.77	5.71
Lu	0.32	0.87	0.57	0.59	0.72	0.62	0.49	0.93	0.87
Mg#	0.61	0.16	0.41	0.51	0.41	0.49	0.59	0.34	0.34
Rb/Sr	0.045	0.802	0.058	0.069	0.012	0.018	0.106	0.043	0.060
Sm/Nd	0.318	0.276	0.231	0.239	0.241	0.215	0.223	0.283	0.285

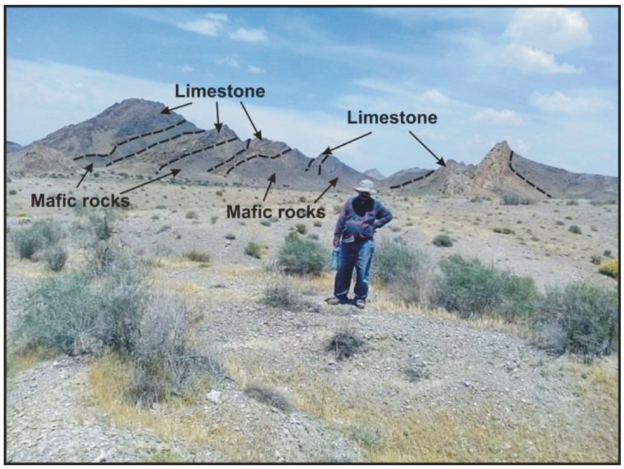

Figure 2. A view of the intercalations of Upper Jurassic–Lower Cretaceous mafic volcanic rocks and limestones in the Dehsard area.

most parts are affected by saussuritization processes and as a result may be transformed into a more sodium-rich variety (albite), although the original shape of the crystal is retained. Chlorite commonly occurs in the groundmass, apparently replacing glass. Pyroxenes also to some extent are affected by hydrothermal alteration and replaced by fibrous amphibole (uralitization processes). In spite of submarine hydrothermal alteration the mafic volcanic rocks maintained their original igneous textures. They experienced two episodes of alteration: the earlier one formed secondary mineral assemblages of the greenschist facies [chlorite, epidote, amphibole (actinolite), quartz, albite, titanite], whereas the later one is noticeable by zeolite and calcite as a sign of zeolite facies. The second phase is obvious by veinlets and uneven masses within the mafic volcanic rocks.

5. Geochemical characteristics

The chemical composition of 26 mafic rocks from the Dehsard area is given in the Table. As it has been delineated above, all samples to some degree were influenced by hydrothermal alteration under zeolite–greenschist facies. The alteration effects are also apparent from the loss on ignition values (LOI = 1.65–6.82 wt %) in the Table, which is a simple way to evaluate the degree of alteration and effect of secondary carbonate and hydrated phases. With the exception of one sample (NO1), the mafic volcanic rocks are less to mildly altered (LOI values at <5 wt %). Thus, considering the mobility of alkali elements during hydrothermal alteration, the use of major element content is unreliable for chemical classification (Pearce and Cann, 1973). Moreover, the variable contents of different incompatible trace elements (e.g., Rb and Sr) signify their redistribution (Cann, 1970). Hence, for the purpose of petrogenetic clarifications it is vital to use elements that remain relatively immobile. It has been argued that through hydrothermal alteration of volcanic rocks the high field strength elements (HFSEs; Ti, P, Zr, Y, Nb, etc.), rare-earth elements (REEs, La to Lu), and transitional metals (e.g., Cr, Ni) are somewhat more immobile in contrast to large ion lithophile elements (LILEs; K, Na, Sr, Rb, Ba, etc.) (Pearce and Cann, 1973; Winchester and Floyd, 1976; Floyd and Winchester, 1978; Pearce, 1996; Özdamar, 2016). Thus, in order to classify Dehsard mafic volcanic rocks the data were plotted on the Zr/TiO_2 versus Nb/Y diagram (Figure 4a), commonly used for classification of altered and metamorphosed volcanic rocks (Winchester and Floyd, 1977; Pearce, 1996). They are mainly basalt and basaltic andesite and show subalkaline characteristic (Figure 4a) in line with petrography studies. Furthermore, their tholeiitic nature is obvious in the TiO_2 versus Zr/P_2O_5 diagram (Figure 4b; Winchester and Floyd, 1976) and also confirmed on the TiO_2 versus Y/Nb plot (not shown) given by Pearce (1975). Moreover, the Dehsard mafic

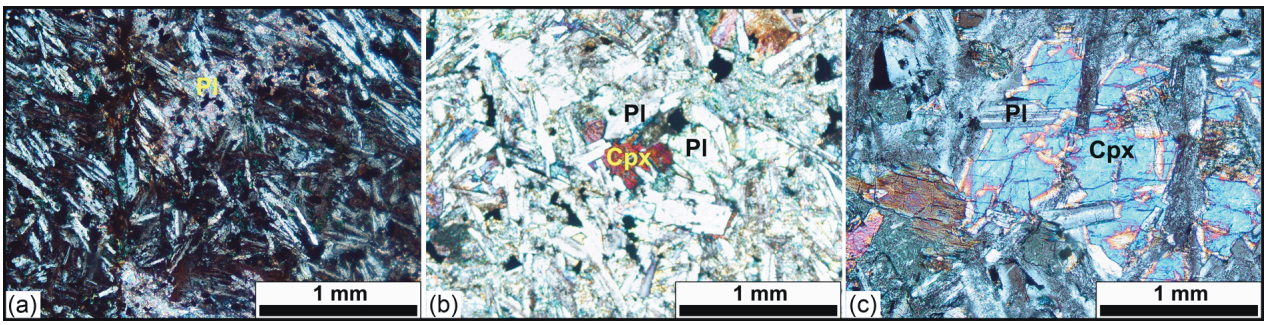

Figure 3. Photomicrographs (in cross polarized light) showing petrographic characteristics of the Dehsard mafic volcanic rocks. (a) basaltic andesite with intergranular and flow textures; (b) basalt with intergranular texture; (c) dolerite with subophitic texture (Cpx: clinopyroxene Pl: plagioclase).

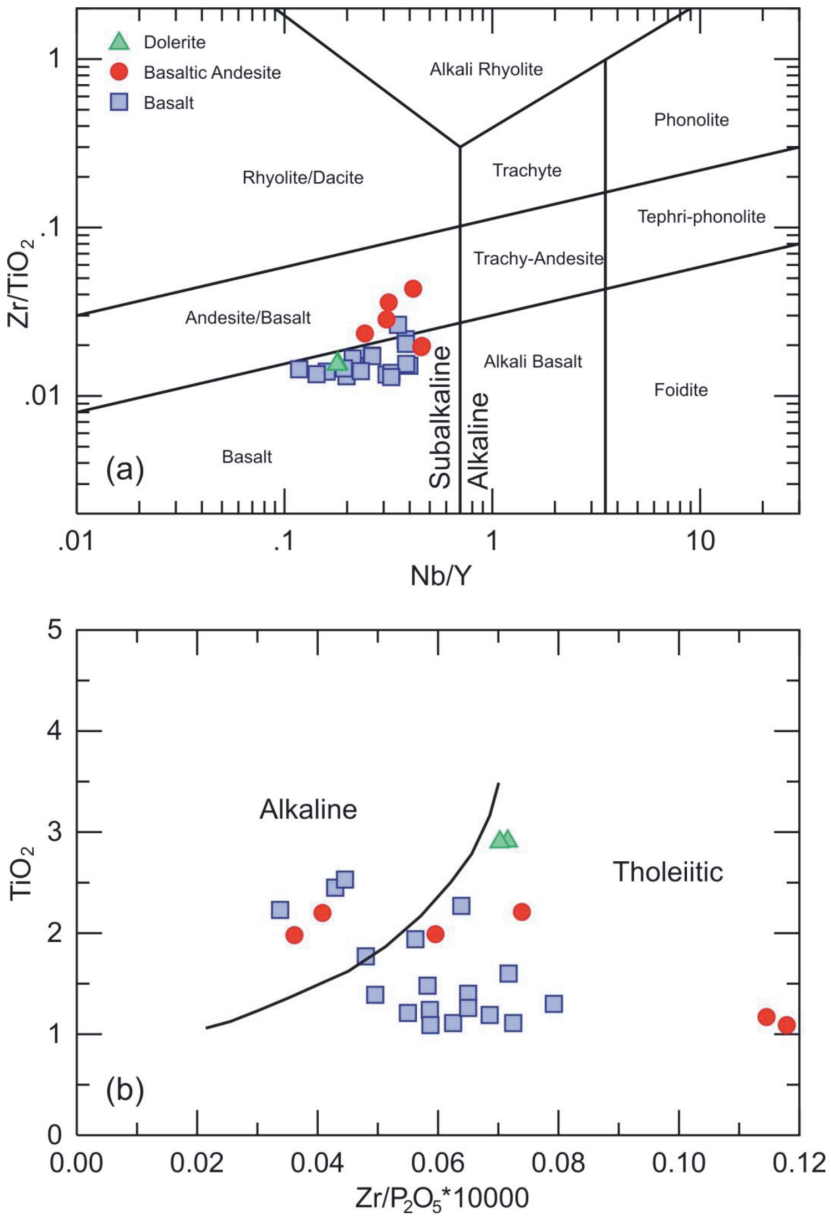

Figure 4. Petrochemical classifications and characteristics of the Dehsard mafic volcanic rocks. (a) Zr/TiO_2 versus Nb/Y [after Winchester and Floyd (1977) modified by Pearce, 1996]; (b) TiO_2 versus $Zr/P_2O_5 \times 10{,}000$ (after Winchester and Floyd, 1976).

volcanic rocks are delineated by the following immobile incompatible trace element ratios: low La/Nb (1.03–2.31) and Nb/Y (0.12–0.46), fairly high Zr/Y (4.03–8.18), Th/Ta (2.25–9.64) and Zr/Nb (12.77–36.15), relatively low TiO_2/P_2O_5 (3.05–9.25), and TiO_2, P_2O_5 contents, which are characteristics of subalkaline (tholeiitic) mafic volcanic rocks (Winchester and Floyd, 1977). As an alteration-independent index for geochemical diversity, Zr concentration implements a good correlation with other elements and can be used to test their mobility (Pearce et al., 1992; Liu et al., 2012b; Wang et al., 2016). Hence, using Zr as a fractionation index, increasing FeO/MgO alongside decreasing MgO, Cr and Ni indicate mafic fractionation (olivine and/or pyroxene) (Figure 5). The positive correlation of Zr with Y and TiO_2 indicates the absence of amphibole and titaniferous oxides (Figure 5). In general, Zr displays a good correlation with HFSEs (shown by Ti and Nb) and REEs (shown by La and Sm), whereas LILEs (displayed by Ba) show scattered distributions, confirming their immobile and mobile characteristics respectively

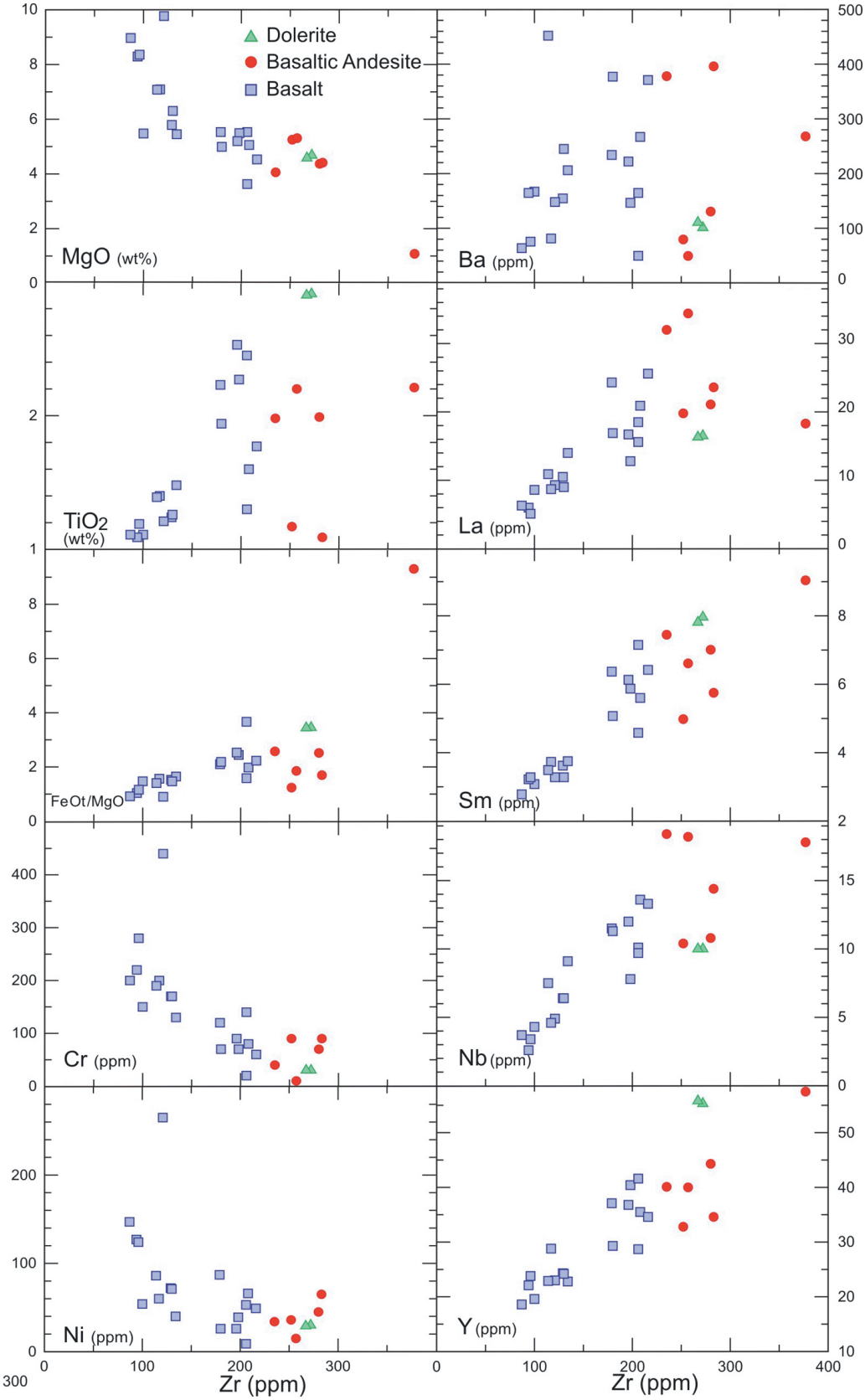

Figure 5. Bivariate plots of Zr (as an index of fractionation) versus selected elements for the Dehsard mafic volcanic rocks.

during the secondary alteration processes (Figure 5). Furthermore, decrease in Cr–Ni and increase in FeO/MgO with Zr and its covariance with other immobile elements can be taken as an indication of the degree of fractionation.

The Dehsard mafic volcanic rocks show relatively strong LREE enrichment and nearly flat HREE patterns on the REE chondrite-normalized diagram (Figure 6) that is commonly distinctive of the island-arc tholeiitic series (Wilson, 1989). They display REE fractionation with La_N/Yb_N = 1.92–5.77, Tb_N/Yb_N = 1.09–1.44, Gd_N/Yb_N = 1.14–1.64, and Eu_N/Eu^* = 0.74–1.15. The negligible or absence of a distinct negative Eu anomaly suggests that

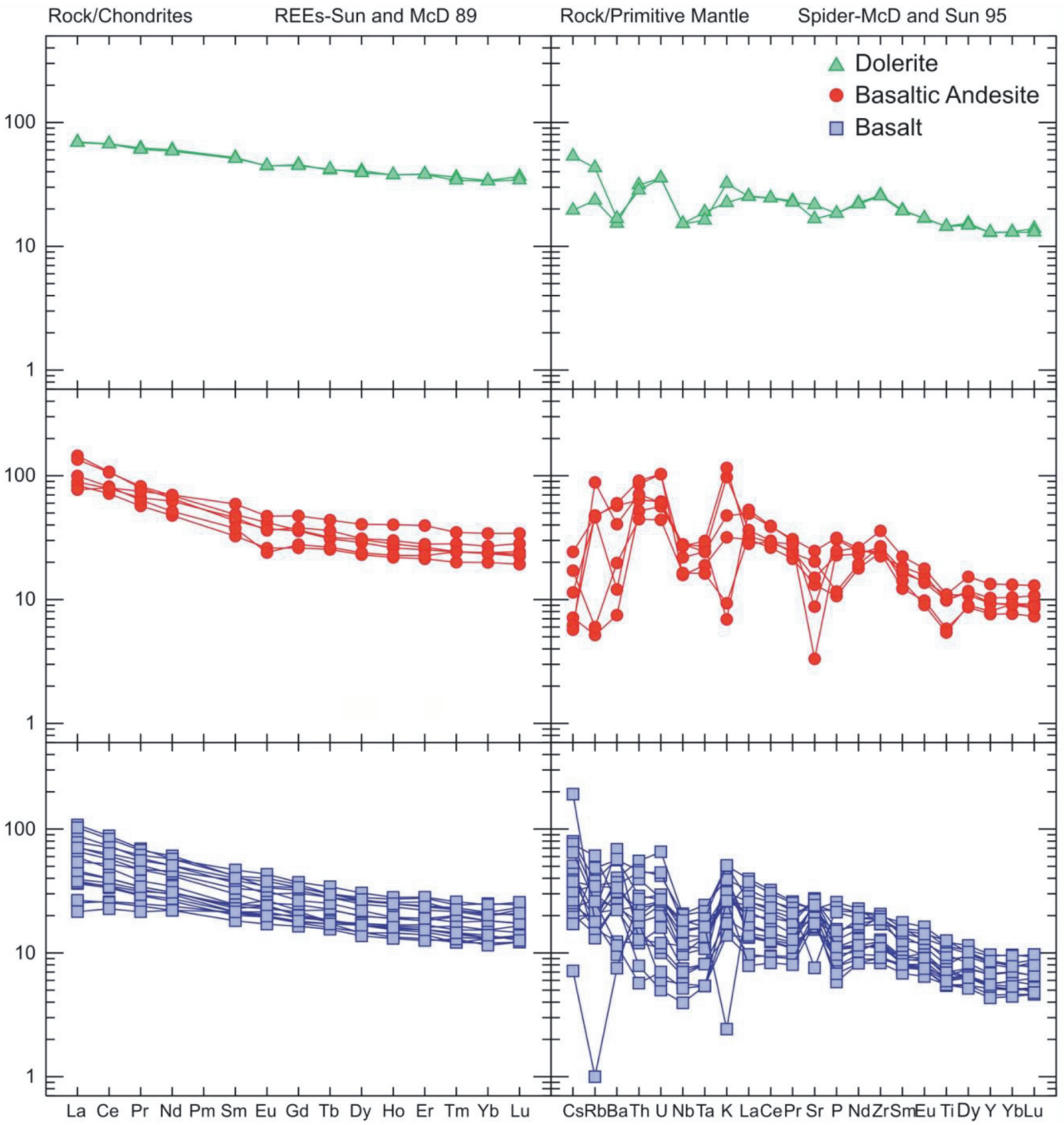

Figure 6. Chondrite-normalized REE patterns (normalizing values are from Sun and McDonough, 1989) and primitive mantle normalized multielement spider diagrams (normalizing values are from McDonough and Sun, 1995) for the Dehsard mafic volcanic rocks.

plagioclase played an insignificant role during magma evolution (Floyd et al., 1991; Slovenec et al., 2010; Qian et al., 2016). The Dehsard mafic volcanic rocks with ratios of Nb/La = 0.47–0.97 and Th/La = 0.09–0.34 and selective enrichment in LILEs (e.g., Ba) and depletion in HFSEs (e.g., Nb, Ta, Ti) on the primitive mantle-normalized multielement spider diagram (Figure 6) indicate an arc volcanic feature (Saunders and Tarney, 1979; Caulfield et al., 2008; Özdamar, 2016).

6. Discussion

6.1. Source of mafic volcanic rocks

In subduction zones the chemical composition of volcanic rocks reveals an input from various components such as fresh and hydrothermally altered oceanic crust, unevenly enriched or depleted material from the mantle wedge, subducted sediments, and fluids and hydrous melts from magmas generated through subduction (Pearce and Parkinson, 1993; Pearce and Peate, 1995; Pearce et al., 1995; Hawkesworth et al., 1997). To identify tectonic environments of basaltic rocks, the HFSEs (such as Ta) and Th are frequently used. In this context, the basalts from subduction zones, in contrast to midoceanic ridge and within-plate basalts, show Th enrichment relative to Ta (Pearce and Peate, 1995). In addition, volcanic rocks in an arc environment have higher LREE/HREE and LILE/HFSE ratios accredited to the incursion of hydrous fluid into the mantle-wedge source and to arrest of elements by fluids derived from the mantle wedge (Hawkesworth et al., 1993; Tatsumi et al., 1995; Gorton and Schandl, 2000). Indeed, the variances in enrichment of some elements in the Dehsard mafic volcanic rocks may demonstrate the path of melting, mantle source, or contamination by crustal source materials. Dehsard mafic volcanic rocks have wide variation in MgO contents (1.08–9.77) and Mg# values (16–66, averaging 48) that are clearly lower than primary magma Mg# values (~70). These composed with their Ni and Cr contents suggest the mantle-derived melts experienced substantial fractionation or intermingling with another material(s) at the magma source (Wilson, 1989; Turner et al., 1992; Class et al., 2000, Özdamar, 2016). The realities that Dehsard mafic volcanic rocks are characterized by similar LREE contents and nearly flat HREE patterns suggest the same magma source (Figure 6). However, in regard to the origin of intermediate volcanic rocks two petrogenetic models have been advocated: (a) as a product of partial melting of mafic to intermediate igneous sources (Rapp and Watson, 1995; Singh and Johannse, 1996; Özdamar, 2016); and (b) by fractional crystallization or assimilation–fractional–crystallization (AFC) processes from a mantle-derived basaltic parental magma (e.g., Pin and Paquette, 1997; Bonin, 2004; Genç and Tüysüz, 2010; Özdamar, 2016). Positive anomaly of Sr, Rb, Ba, and K and negative anomaly of Nb and Ta (Figure 6) and decreases in ratios of Zr/Nb and Y/Nb together with the observed trend in Figure 7a all reveal subduction zone magmatism for Dehsard mafic volcanic rocks (Cox and Hawkesworth, 1985; Özdamar, 2016). Their relative enrichment of Th and LREEs in respect to HFSEs shows possible derivation from a mantle source that was modified by slab-derived components. In addition, Th/La ratios (0.09–0.34) in the Dehsard mafic volcanic rocks are analogous to that of arc basalts (Plank, 2005). It has also been indicated that the REEs (La/Yb ratios) are informant for the pressure-sensitive residual minerals and melting percentages of the source (Kay et al., 1991, 1994; Haschke and Gunthner, 2003). They argued that high La/Yb ratios (>20) show more HREEs retaining (such as Yb) by garnet and amphibole in the residue, whereas lower La/Yb ratios mostly specify lower-pressure conditions. The La/Yb ratios (averaging 4.72) in the Dehsard mafic volcanic rocks show the nonexistence of garnet as a residual phase in the source region. The plot of La_N/Yb_N versus La_N/Sm_N (not shown) (Ma et al., 2014) indicates the magmas parental to the Dehsard mafic volcanic rocks were derived from the spinel peridotite source region.

In the Ba/La versus Th/Yb diagram (Figure 7b), the samples show almost constant Th/Yb ratios with increasing Ba/La, indicating the contribution of slab-derived fluids in the mantle source. Also in the Nb/Th versus La/Nb diagram (Figure 7c) most of the samples plot in the field of arc volcanic rocks or magmas that may have been polluted by crustal source components (Pearce, 1983; Wang et al., 2016). The plot of Dehsard mafic volcanic rocks in the Nb/Ta versus Nb diagram (Figure 7d) clearly shows the role of fractional crystallization trend and the input of sediment constituent in the magma origin (Caulfield et al., 2008; Wang et al., 2016). In addition, the La/Nb ratio greater than 1 in the Dehsard mafic volcanic rocks suggests their derivation from a lithospheric mantle source (DePaolo and Daley, 2000; Etruk et al., 2017). Furthermore, the plots of least evolved samples of the Dehsard mafic volcanic rocks (samples having high MgO content >6%) in the Sm/Yb versus La/Yb diagram (Liu et al., 2014) (Figure 8) show that they resulted from 3%–10% partial melting of spinel lherzolite with primitive mantle starting composition. This has been confirmed in the Dy_N/Yb_N versus $(Yb)_N$ diagram (not shown) given by Çolakoğlu et al. (2014). Thus, as discussed above both FC and AFC processes together with contamination by crustal source materials and slab-derived fluids were involved in the evolution of Dehsard mafic volcanic rocks.

6.2. Tectonic implication

The distinct negative Nb and Ta anomalies in the Dehsard mafic volcanic rocks (Figure 6) are typical of magma generated at subduction zones (Pearce, 1983). Their

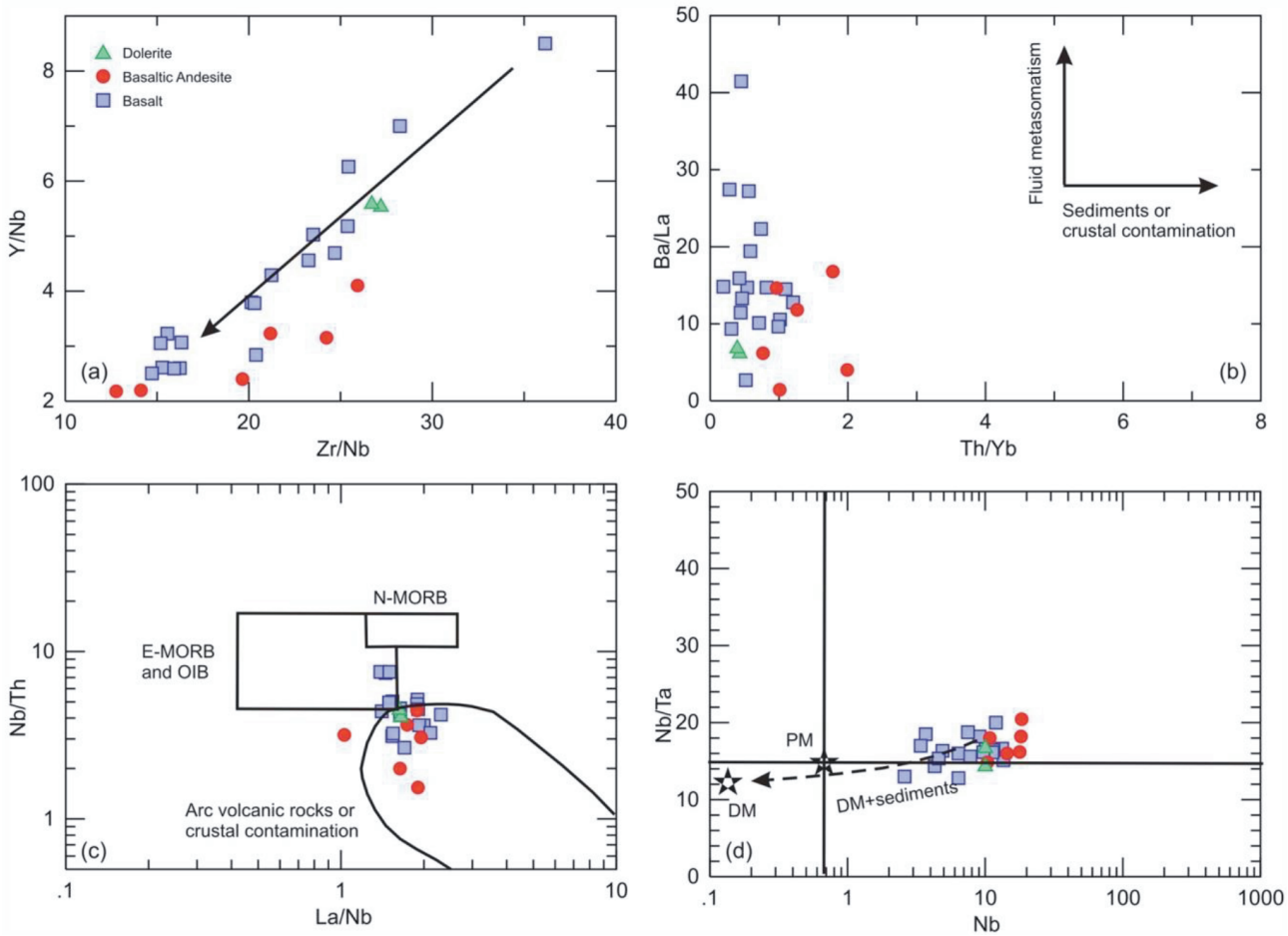

Figure 7. Bivariate plots of (a) Y/Nb versus Zr/Nb, (b) Ba/La versus Th/Yb, (c) Nb/Th versus La/Nb, (d) Nb/Ta versus Nb for the Dehsard mafic volcanic rocks. DM = Depleted Mantle, PM = Primitive Mantle, OIB = Oceanic Island Basalt.

average of Nb/Ta = 16.45 is also in the range of Nb/Ta values reported for fairly depleted island-arc volcanic rocks (Nb/Ta ~ 17) (Stolz et al., 1996). The distinctive subduction (and/or crustal) signature represented also by selective enrichment in LILE and LREE with respect to the HFSE and has been related to the dehydration of the altered oceanic crust (or the subducted sediments) or the partial melting of the altered oceanic crust (or the subducted sediments) (Keskin et al., 1998; Oyan et al., 2016). Furthermore, the island arc characteristic of Dehsard mafic volcanic rocks is shown in the La/Yb versus Th/Yb diagram given by Condie (1989) (Figure 9a). Moreover, in the Th-Ta-Hf/3 discrimination diagram nearly all the samples plot in the field of calc-alkaline volcanic arc basalts and back-arc basin basalts (BABBs) supplementary field (Figure 9b) (Wood, 1980; Floyd et al., 1991). It has been shown that some BABBs in the mature subduction zone can have transitional chemical aspect to calc-alkaline basalts and distinctive higher LILE/HFSE ratios (Saunders and Tarney, 1984; Floyd et al., 1991). In discrimination of the tectonic setting, using V versus Ti/1000 reported by Shervais (1982) and Zr/Y versus Zr given by Pearce and Norry (1979), almost all Dehsard mafic volcanic rocks plot in the field of MORB + BABB and WPB, respectively (Figures 9c and 9d). It has been argued that La/Nb versus Y is a suitable discrimination diagram between ocean ridge and subduction related eruptive settings (Cameron et al., 1980; Floyd et al., 1991). The modest value of La/Nb ratios (in average 1.70) of the Dehsard mafic volcanic rocks show their back-arc basin characteristics (rather than an arc) that is recognizable from enriched MORB or intraplate oceanic lava flows with similar low Y contents (Figure 10a) (Floyd, 1989; Floyd et al., 1991). Furthermore, their back arc basin origin is evident in the Ti/Zr versus Zr diagram (Figure 10b) (Woodhead et al., 1993, Bagas et al., 2008). Furthermore, in the tectonic diagrams for volcanic rocks classification (Schandl and Gorton, 2002) all samples plot in the field of WPVZ (within-plate volcanic zone) with minor tendency toward active continental margin, which points to an extensional phase volcanism (Figure 11). This

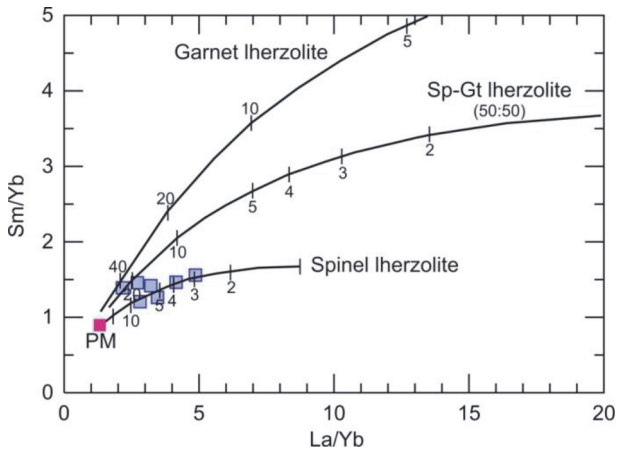

Figure 8. Sm/Yb versus La/Yb diagram (after Liu et al., 2014) for the Dehsard mafic volcanic rocks. PM = Primitive Mantle. Only least evolved samples having high MgO content >6% were plotted.

together with within plate characteristic in the Zr/Y versus Zr diagram (Figure 9d) is not in conflict with Dehsard mafic volcanic rocks back-arc settings. Indeed, it has been specified that the back-arc basin is a place where various chemical types of basalts can be found, including BABB-, IAB-, N-MORB-, E-MORB-, and OIB-like signatures (Leat et al., 2000, 2004; Pearce et al., 2005; Hickey-Vargas et al., 2006; Sayit et al., 2016). Beccaluva et al. (2004) also point to IAT/MORB intermediate features of back-arc basin basalt. They argue that intraoceanic subduction within original MORB-type lithosphere could create supra-subduction basaltic magmatism with island arc tholeiitic affinity and formation of an incipient arc. Undoubtedly, the important difference between BABB and MORB is the participation of slab-derived components to variable extents in the BABB that influence its petrogenesis (Pearce and Stern, 2006; Sayit et al., 2016). Therefore, in terms of presented tectonic discrimination diagrams and geochemical composition an

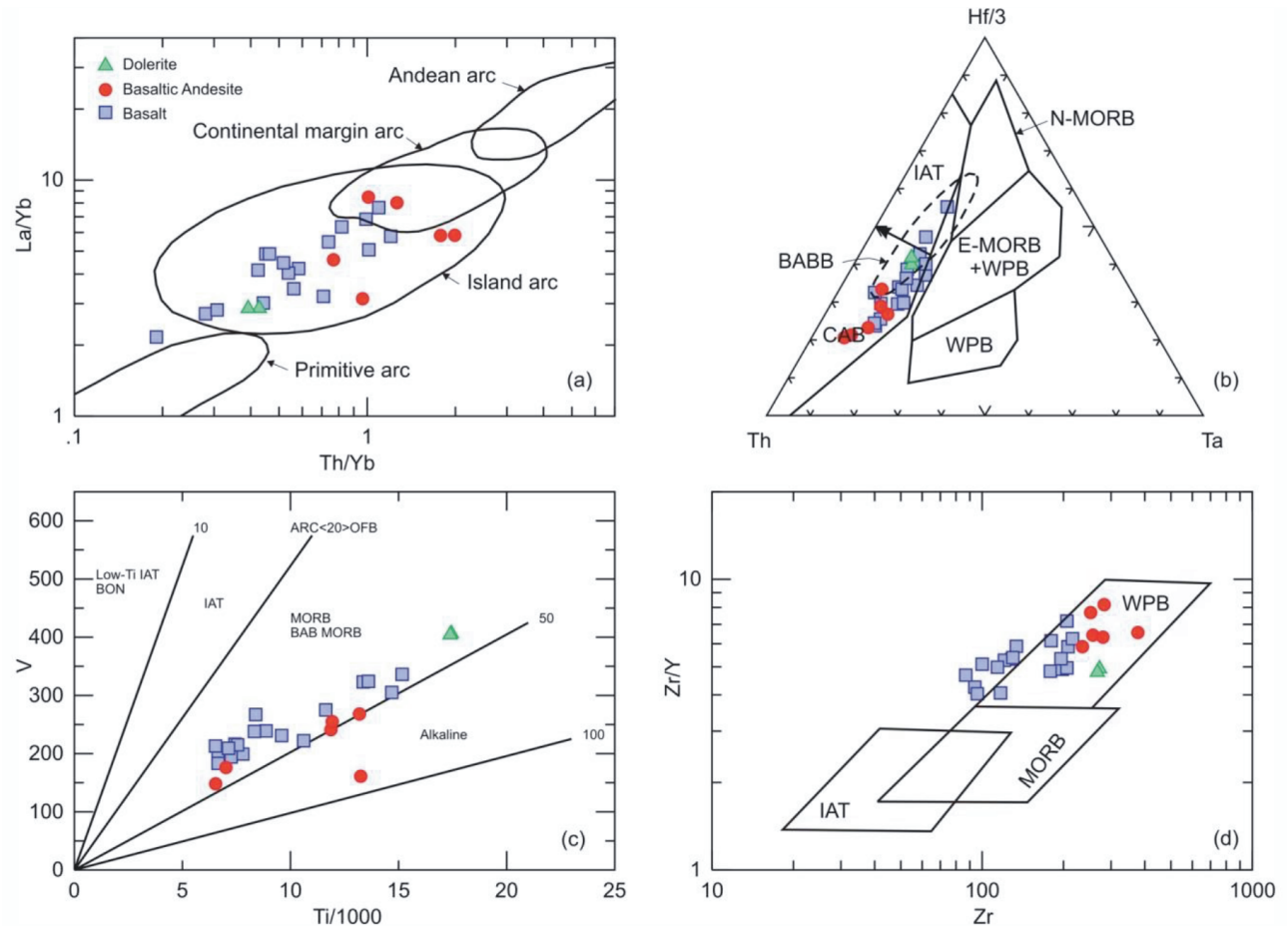

Figure 9. Tectonic discrimination plots for the Dehsard mafic volcanic rocks. (a) La/Yb versus Th/Yb (Condie, 1989), (b) Hf/3-Th-Ta (Wood, 1980), Back-arc basin field (BABB) from Floyd et al., 1991, (c) V versus Ti/1000 (Shervais, 1982), (d) Zr/Y versus Zr (Pearce and Norry, 1979). Abbreviations; BABB, Back Arc Basin Basalts, E-MORB, Enriched Mid-Oceanic Ridge Basalts, IAT, Island Arc Tholeiites, MORB, Mid-Oceanic Ridge Basalts, WPB, Within Plate Basalt.

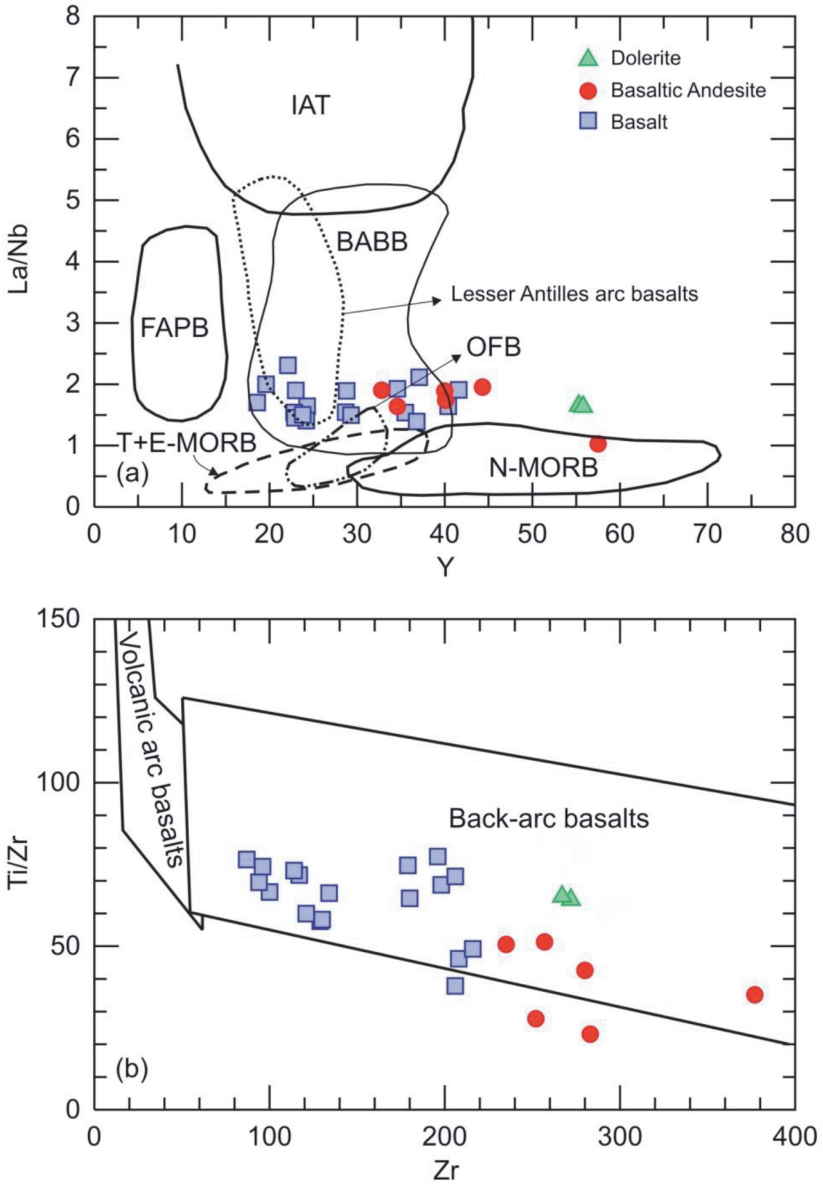

Figure 10. Discrimination of BABB affinity of the Dehsard mafic volcanic rocks on: (a) La/Nb versus Y (Floyd et al., 1991), (b) Ti/Zr versus Zr (Woodhead et al., 1993). Abbreviations; BABB, Back Arc Basin Basalts, FAPB, Fore-Arc Platform Basalts, IAT, Island Arc Tholeiites, MORB, Mid-Oceanic Ridge Basalts, OFB, Oceanic Flood Basalts.

arc setting and/or probable back-arc basin environment can be considered for the Dehsard mafic volcanic rocks. A similar setting has been also suggested for the initiation of Middle to Late Jurassic island arc (Songhor arc) and back-arc basin in northwest Iran (resulted from the northward subduction of the Neo-Tethys ocean), which led to the development of Songhor–Ghorveh mafic to intermediate volcanic rocks (Azizi and Asahara, 2013). Furthermore, it is thought that after the beginning of the northern subduction of the Neo-Tethys oceanic lithosphere underneath the southern margin of the Central Iranian Microcontinents, a newly formed back-arc basin developed in the north. Consequently, the back-arc basin was affected by small volume slab-released fluids/melts and largely subback-arc mantle-derived melts with MORB- or IAT-like affinity (Shaker Ardakani et al., 2009; Rajabzadeh et al., 2013).

7. Conclusion

The Dehsard mafic volcanic rocks with probable age of Late Jurassic–Early Cretaceous are outcropped in

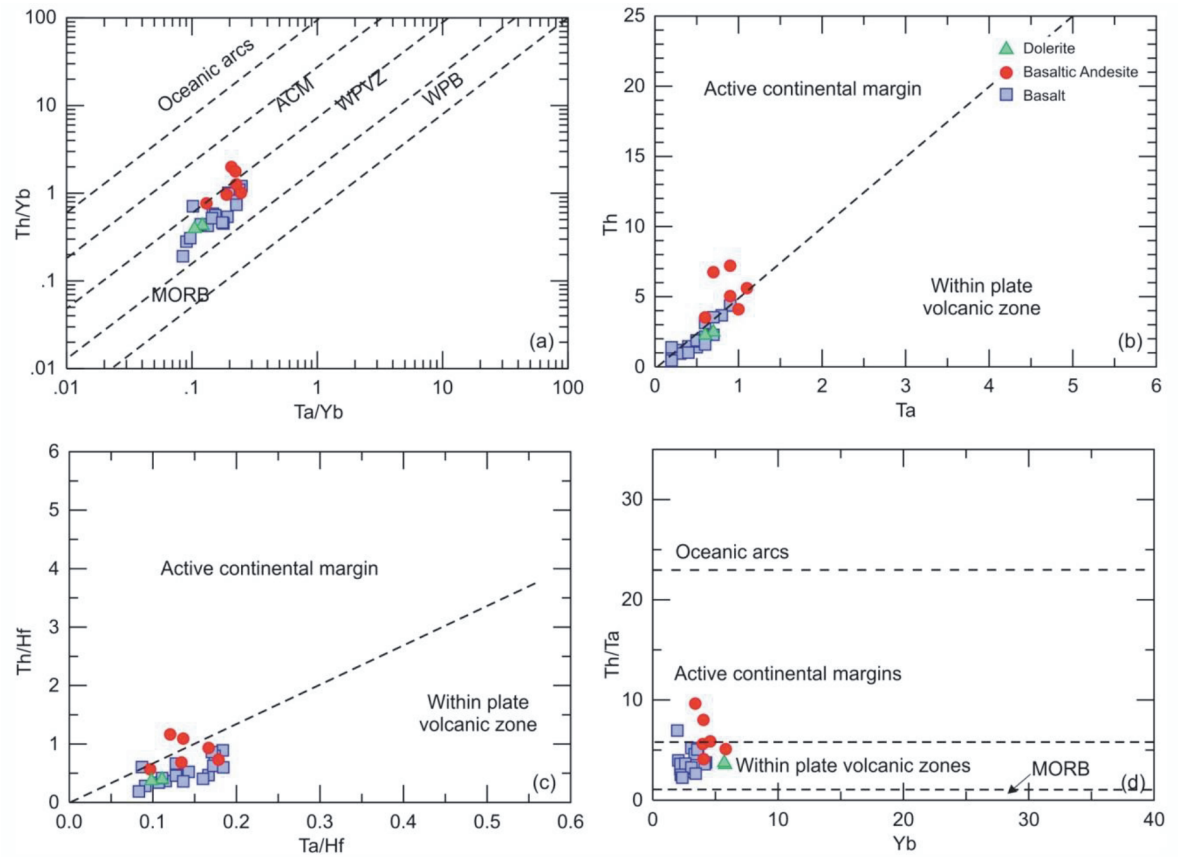

Figure 11. Tectonic setting diagrams for the Dehsard mafic volcanic rocks (after Schandl and Goroton, 2002). Abbreviations; ACM, Active Continental Margin, MORB, Mid-Oceanic Ridge Basalt, WPB, Within Plate Basalt, WPVZ, Within Plate Volcanic Zone.

the southernmost part of the Sanandaj–Sirjan Zone. They consist mainly of basalt and basaltic andesite with subordinate dolerite. They show mostly analogous patterns with relatively strong LREE and LILE enrichment, HFSE (e.g., Nb, Ta, Ti) depletion, and almost flat HREE shapes. Their minor or absence of negative Eu anomalies and La/Yb ratios suggest that plagioclase played a negligible role during magma evolution and nonexistence of residual garnet phase in the source region, respectively. Positive Sr, Rb, Ba, and K and negative Nb and Ta anomalies together with decreases in Zr/Nb and Y/Nb ratios are characteristic of subduction zone magmatism. Our geochemical data also back this interpretation that the Dehsard mafic magma is derived from partial melting of a depleted mantle source in an arc environment (most seemingly back-arc basin) that experienced fractional crystallization and AFC together with contamination by melts of subducted sediments. Overall data show that the Dehsard mafic volcanic rocks have similarities to back-arc basin environment, with low La/Nb (1.03–2.31) and Nb/Y (0.12–0.46), relatively high Zr/Y (4.03–8.18) and Th/Ta (2.25–9.64) ratios, modest La/Nb ratio, and progressively enriched normalized patterns. We contemplate that the arc-related Dehsard mafic volcanic rocks were erupted in an island arc setting (Dehsard island arc) that resulted from development of an intraoceanic subduction in the Neo-Tethyan oceanic crust prior to the Late Jurassic–Early Cretaceous as it was subducting northward under the southern margin of the Central Iranian Microcontinents. The later collision of the arc with SSZ led to tectonic proximity of the Dehsard mafic volcanic rocks to SSZ components. This finding provides new insights for the reconstruction of the geodynamic history of the Sanandaj–Sirjan zone.

Acknowledgments

This work is part of the PhD research project of the first author. A portion of the research fund was provided by Ministry of Science, Research and Technology of Iran through the Vice Chancellor for Research and Technology at Shahid Bahonar University of Kerman. The authors gratefully acknowledge Dr. Irfan Temizel and two anonymous reviewers for their critical and constructive reviews and comments that improved the quality of our manuscript.

References

Agard P, Omrani J, Jolivet L, Mouthereau F (2005). Convergence history across Zagros (Iran): Constraints from collisional and earlier deformation. Int J Earth Sci 94: 401–419, doi:10.1007/s00531-005-0481-4.

Ahmad T, Posht Kuhi M (1993). Geochemistry and petrogenesis of Urumiah-Dokhtar volcanic belt around Nain and Rafsanjan areas: a preliminary study. Treatise on the geology of Iran. Iranian Ministry of Mines and Metals, p. 90.

Ahmadi Khalaji A, Esmaeily D, Valizadeh MV, Rahimpour-Bonab H (2007). Petrology and geochemistry of the granitoid complex of Boroujerd, Sanandaj–Sirjan Zone, Western Iran. J Asian Earth Sci 29: 859-877.

Alavi M (2004). Regional stratigraphy of the Zagros folded-thrust belt of Iran and its proforeland evolution. Am J Sci 304: 1-20.

Amiri M, Ahmadi Khalaji A, Tahmasbi Z, Santos JF, Zarei Sahamieh R, Zamanian H (2017). Geochemistry, petrogenesis, and tectonic setting of the Almogholagh batholith in the Sanandaje–Sirjan zone, western Iran. J African Earth Sci 134: 113-133.

Arvin M, Pan Y, Dargahi S, Malekizadeh A, Babaei A (2007). Petrochemistry of the Siah–Kuh granitoid stock southwest of Kerman, Iran: implications for initiation of Neotethys subduction. J Asian Earth Sci 30: 474-489.

Azizi H, Asahara Y (2013). Juvenile granite in the Sanandaj–Sirjan Zone, NW Iran: late Jurassic–Early Cretaceous arc–continent collision. Int Geol Rev 55: 1523-1540.

Bagas L, Bierlein FP, English L, Anderson JAC, Maidmentd D, Hustond DL (2008). An example of a Palaeoproterozoic back-arc basin: petrology and geochemistry of the ca. 1864Ma Stubbins Formation as an aid towards an improved understanding of the Granites–Tanami Orogen, Western Australia. Precamb Res 166: 168-184.

Baharifar A, Moinevaziri H, Bellon H, Piqué A (2004). The crystalline complexes of Hamadan (Sanandaj–Sirjan zone, western Iran): metasedimentary Mesozoic sequences affected by Late Cretaceous tectono-metamorphic and plutonic events. Compt Rend Geosci 336: 1443-1452.

Beccaluva L, Coltorti M, Giunta G, Siena F (2004). Tethyan vs. Cordilleran ophiolites: a reappraisal of distinctive tectono-magmatic features of supra-subduction complexes in relation to the subduction mode. Tectonophysics 393: 163-374.

Berberian F, Berberian M (1981). Tectono-plutonic episodes in Iran. In: Gupta HK, Delany FM, editors. Zagros, Hindu Kush, Himalaya, geodynamic evolution: Geodynamic Series 3, Working Group 6, Am Geophys Union, pp. 5-32.

Berberian M, King GC (1981). Towards a paleogeography and tectonics evolution of Iran. Can J Earth Sci 18: 210-265.

Berberian F, Muir ID, Pankhurst RJ, Berberian M (1982). Late Cretaceous and early Miocene Andean-type plutonic activity in northern Makran and central Iran. J Geol Soc London 139: 605-614.

Bonin B (2004). Do coeval mafic and felsic magmas in post-collisional to within-plate regimes necessarily imply two contrasting, mantle and crustal, sources? A review. Lithos 78: 1-24.

Cameron WE, Nisbet EG, Dietrich VJ (1980). Petrographic dissimilarities between ophiolitic and ocean-floor basalts. In: Panayiotou A, editor. Ophiolites. Proc Internat Ophiolite Symp Geol Surv Dept Cyprus Nicosia, pp. 182-192.

Cann JR (1970). Rb, Sr, Y, Zr and Nb in some ocean floor basaltic rocks. Earth Planet Sci Lett 10: 7-11.

Caulfield JT, Turner SP, Dosseto A, Pearson NJ, Beier C (2008). Source depletion and extent of melting in the Tongan sub-arc mantle. Earth Planet Sci Lett 273: 279-288.

Class C, Miller DM, Goldstein SL, Langmuir CH (2000). Distinguishing melt and fluid subduction components in Umnak Volcanics, Aleutian Arc. Geochem Geophys Geosyst 1, doi.org/10.1029/1999GC000010.

Condie KC (1989). Geochemical changes in basalts and andesites across the Archean Proterozoic boundary: identification and significance. Lithos 23: 1-18.

Cox KG, Hawkesworth CJ (1985). Geochemical stratigraphy of the Deccan Traps at Mahabaleshwar, Western Ghats, India, with implications for open system magmatic processes. J Petrol 26: 355-377.

De Paolo DJ, Daley EE (2000). Neodymium isotopes in basalts of the southwest basin and range and lithospheric thinning during continental extension. Chem Geol 169: 157-185.

Esna-Ashari A, Tiepolo M, Valizadeh MV, Hassanzadeh J, Sepahi AA (2012). Geochemistry and zircon U-Pb geochronology of Aligoodarz granitoid complex, Sanandaj-Sirjan zone, Iran. J Asian Earth Sci 43: 11-22.

Erturk MA, Beyarslan M, Chung SL, Lin TH (2017). Eocene magmatism (Maden Complex) in the Southeast Anatolian Orogenic Belt: Magma genesis and tectonic implications. Geos Front https://doi.org/10.1016/j.gsf.2017.09.008.

Fergusson CL, Nutman AP, Mohajjel M, Bennett VC (2016). The Sanandaj–Sirjan Zone in the Neo-Tethyan suture, western Iran: Zircon U–Pb evidence of late Palaeozoic rifting of northern Gondwana and mid-Jurassic orogenesis. Gondwana Res 40: 43-57.

Floyd PA (1989). Geochemical features of intraplate oceanic plateau basalts. In: Saunders A, Norry M, editors. Magmatism in ocean basins. Geol Soc London Spec Publ 42: 215-230.

Floyd PA, Kelling G, Gocken SL, Gocken N (1991). Geochemistry and tectonic environment of basaltic rocks from the Miss ophiolitic melange, south Turkey. Chem Geol 89: 263-280.

Floyd PA, Winchester JA (1978). Identification and discrimination of altered and metamorphosed volcanic rocks using immobile elements. Chem Geol 21: 291-306.

Förster H, Fesefeldt K, Kürsten M (1972). Magmatic and orogenic evolution of the central Iranian volcanic belt. In 24th International Geologic Congress, edited by Armstrong JE Hedberg HD, Int Geol Congr Montreal QC Canada, pp. 198-210.

Genç ŞC, Tüysüz O (2010). Tectonic setting of the Jurassic bimodal magmatism in the Sakarya Zone (Central and Western Pontides), Northern Turkey: a geochemical and isotopic approach. Lithos 118: 95-111.

Çolakoğlu AL, Günay K, Göncüoğlu MC, Oyan V, Erdoğan K (2014). Geochemical evaluation of the late Maastrichtian subduction-related volcanism in the southern Neotethys in Van area, and a correlation across the Turkish-Iranian border. Ofioliti 39: 51-65.

Gorton MP, Schandl ES (2000). From continents to island arcs: a geochemical index of tectonic setting for arc-related and within-plate felsic to intermediate volcanic rocks. Can Mineral 38: 1065-1073.

Haschke M, Gunther A (2003). Balancing crustal thickening in arcs by tectonic vs magmatic means. Geology 31: 933-936.

Hawkesworth CJ, Gallagher K, Hergt JM, McDermott F (1993). Mantle slab contributions in arc magmas. Annu Rev Earth Planet Sci 21: 175-204.

Hawkesworth CJ, Turner SP, McDermott F, Peate DW van Calsteren P (1997). U-Th isotopes in arc magmas: implications for element transfer from the subducted crust. Science 276: 551-555.

Hickey-Vargas R, Savov I, Bizimis M, Ishii T, Fujioka K (2006). Origin of diverse geochemical signatures in igneous rocks from the West Philippine Basin: implications for tectonic models. In: Christie D, editor. Back-arc spreading systems: geological, biological, chemical and physical interactions. AGU Geophys Monog Ser 166: 287-303.

Jung D, Kursten M, Tarakian M (1976). Post-Mesozoic Volcanism in Iran and Its Relation to the Sub-Duction of the Afro-Arabian under the Eurasian Plate. In: Pilger A, Rosler A, editors. Afar between Continental and Oceanic Rifting, Volume II, Stuttgart, Germany: Schweizerbatsche Verlagsbuch-Handlung, pp. 175-181.

Kay SM, Mpodozis C, Ramos VA, Munizaga F (1991). Magma source variations for mid-Tertiary magmatic rocks associated with a shallowing subduction zone and a thickening crust in the Central Andes (288–338S). In Harmon RS, Rapela CW, editors. Andean magmatism and its tectonic setting. Geol Soc Am Spec Publ 265: 113-137.

Kay SM, Mpodozis C, Tittler A, Cornejo P (1994). Tertiary magmatic evolution of the Maricunga mineral belt in Chile. Int Geol Rev 36: 1079-1112.

Keskin M, Pearce JA, Mitchell JG (1998). Volcano-stratigraphy and geochemistry of collision-related volcanism in the Erzurum-Kars plateau, northeastern Turkey. J Volcanol Geotherm Res 85: 355-404.

Leat PT, Livermore RA, Millar IL, Pearce JA (2000). Magma supply in back-arc spreading centre segment E2, East Scotia Ridge. J Petrol 41: 845-866.

Leat PT, Pearce JA, Barker PF, Millar IL, Barry TL, Larter RD (2004). Magma genesis and mantle flow at a subducting slab edge: the South Sandwich arc-basin system. Earth Planet Sci Lett 227: 17-35.

Liu B, Ma CQ, Zhang JY, Xiong FH, Huang J, Jiang HA (2014). ^{40}Ar–^{39}Ar age and geochemistry of subduction-related mafic dikes in northern Tibet, China: petrogenesis and tectonic implications. Int Geol Rev 56: 57-73.

Liu SW, Zhang J, Li QG, Zhang LF, Wang W, Yang PT (2012b). Geochemistry and U– Pb zircon ages of metamorphic volcanic rocks of the Paleoproterozoic Lüliang Complex and constraints on the evolution of the Trans-North China Orogen, North China Craton. Precamb Res 222: 173-190.

Ma X, Chen B, Chen JF, Qu WJ (2014). Petrogenesis and geodynamic significance of the late Palaeozoic Dongwanzi Complex, North China Craton: constraints from petrological, geochemical, and Os-Nd-Sr isotopic data. Int Geol Rev 56: 1521-1540.

McDonough WF, Sun SS (1995). The composition of the Earth. Chem Geol 120: 223-253.

McKenzie D, O'Nions RK (1991). Partial melt distributions of rare earth element concentrations. J Petrol 32: 1021-1091.

Mohajjel M, Fergusson CL (2000). Dextral transpression in late Cretaceous continental collision, Sanandaj-Sirjan Zone, Western Iran. J Struct Geol 22: 1125-1139.

Mohajjel M, Fergusson CL, Sahandi MR (2003). Cretaceous– Tertiary convergence and continental collision, Sanandaj- Sirjan Zone, western Iran. J Asian Earth Sci 21: 397–412.

Nazemzadeh M, Rashidi A (2006). Geological map of the Dehsard (Bezar), Scale 1/100,000. Geological Survey of Iran, Sheet No. 7347.

Oyan V, Keskin M, Lebedev VA, Chugaev AV, Sharkov E (2016). Magmatic evolution of the Early Pliocene Etrüsk stratovolcano, eastern Anatolian collision zone, Turkey. Lithos 256-257: 88-108.

Özdamar S (2016). Geochemistry and geochronology of late Mesozoic volcanic rocks in the northern part of the Eastern Pontide Orogenic belt (NE Turkey): implications for the closure of the Neo-Tethyan Ocean. Lithos 248-251: 240-256.

Pearce JA (1975). Basalt geochemistry used to investigate past tectonic environments on Cyprus. Tectonophysics 25: 41-68.

Pearce JA (1982). Trace element characteristics of lavas from destructive plate boundaries. In: Thorpe RS, editor. Andesites. New York, NY, USA: Wiley, pp. 525-548.

Pearce JA (1983). Role of the subcontinental lithosphere in magma genesis at active continental margins. In: Hawkesworth CJ, Norry MJ, editors. Continental Basalts and Mantle Xenoliths. Nantwich, UK: Shiva Press, pp. 230-249.

Pearce JA (1996). A user's guide to basalt discrimination diagrams. In: Wyman DA, editor. Trace Element Geochemistry of Volcanic Rocks; Applications for Massive Sulphide Exploration. Geol Assoc Canada Short Course Notes 12, pp. 79-113.

Pearce JA, Baker PE, Havery PK, Luff IW (1995). Geochemical evidence for subduction fluxes, mantle melting and fractional crystallization beneath the South Sandwich island arc. J Petrol 36: 1073-1109.

Pearce JA, Cann JR (1973). Tectonic setting of basic volcanic rocks determined using trace element analyses. Earth Planet Sci Lett 12: 339-349.

Pearce JA, Lippard SJ, Roberts S (1984). Characteristics and tectonic significance of supra-subduction zone ophiolites. In: Kolelaar BP, Howells MF, editors. Marginal basin geology. Geol Soc London Spec Publ 16: 77-94.

Pearce JA, Norry MJ (1979). Petrogenetic implications of Ti, Zr, Y and Nb variations in volcanic rocks. Contrib Mineral Petrol 69: 33-47.

Pearce JA, Parkinson IJ (1993). Trace element models for mantle melting: application to volcanic arc petrogenesis. In: Prichard HM, Alabaster T, Harris NBW, Neary CR, editors. Magmatic Processes and Plate Tectonics. Nantwich, UK: Shiva Press, pp. 373-403.

Pearce JA, Peate DW (1995). Tectonic implications of the composition of volcanic arc magmas. Annu Rev Earth Planet Sci 23: 251-286.

Pearce JA Stern RJ (2006). Origin of back-arc basin magmas: trace element and isotope perspectives. In: Christie D, editor. Back-arc spreading systems: geological, biological, chemical and physical interactions. AGU Geophy Monog Ser 166: 63-86

Pearce JA, Stern JA, Bloomer SH, Fryer P (2005). Geochemical mapping of the Mariana arc-basin system: implications for the nature and distribution of subduction components. Geochem Geophys Geosyst 6, Q07006, doi:10.1029/2004GC000895.

Pearce JA, van der Laan SR, Arculus RJ, Murton BJ, Ishii T, Peate DW, Parkinson IJ (1992). Boninite and harzburgite from Leg 125 (Bonin–Mariana forearc): a case study of magma genesis during the initial stages of subduction. Proc Ocean Drill Prog Sci Results pp. 623-659.

Pin C, Paquette JL (1997). A mantle-derived bimodal suite in the Hercynian belt: Nd isotope and trace element evidence for a subduction-related rift origin of the late Devonian Brevenne metavolcanics, Massif Central (France). Contrib Mineral Petrol 129: 222-238.

Plank T (2005). Constraints from Thorium/Lanthanum on sediment recycling at subduction zones and the evolution of the continents. J Petrol 46: 921-944.

Qian X, Wang Y Feng Q, Wei ZiJ, Zhang Y, Chonglakmani C (2016). Petrogenesis and tectonic implication of the Late Triassic post-collisional volcanic rocks in Chiang Khong, NW Thailand. Lithos, 248-251: 418-431.

Rajabzadeh MA, Dehkordi TN, Caran S (2013). Mineralogy, geochemistry and geotectonic significance of mantle peridotites with high-Cr chromitites in the Neyriz ophiolite from the outer Zagros ophiolite belts, Iran. J African Earth Sci 78: 1-15.

Rapp RP, Watson EB (1995). Dehydration melting of metabasalt at 8-32 kbar: implications for continental growth and crust-mantle recycling. J Petrol 36: 891-931.

Sabzehei M (1994). Geological map of the Hajiabad, Scale 1/250,000. Geological Survey of Iran, Quadrangle No. 112.

Saunders AD, Tarney J (1979). The geochemistry of basalts from a back-arc spreading centre in the east Scotia Sea. Geochim Cosmochim Acta 43: 555-572.

Saunders AD, Tarney J (1984). Geochemical characteristics of basaltic volcanism within back-arc basins. In: Kloeaar BP, Howells MF, editors. Marginal basin geology. Geol Soc London Spec Publ 16: 59-76.

Sayit K, Marroni M, Göncüoglu MC, Pandolfi L, Ellero A, Ottria G, Frassi C (2016). Erratum to: Geological setting and geochemical signatures of the mafic volcanic rocks from the Intra-Pontide Suture Zone: implications for the geodynamic reconstruction of the Mesozoic Neotethys. Int J Earth Sci (Geol Rundsch) 105: 39-64.

Schandl ES, Gorton MP (2002). Application of high field strength elements to discriminate tectonic settings in VMS environments. Econ Geol 97: 629-642.

Schroeder JW (1944). Essai sur la structure de l'Iran. Eclogae Geol Helv 37: 37-81 (in French).

Sedighian S, Dargahi S, Arvin M (2017). Petrochemistry of Khunrang intrusive complex, southeast of Kerman, Iran: implications for magmatic evolution of Sanandaj-Sirjan zone in the Mesozoic time. J African Earth Sci 134: 149-165.

Şengör AMC, Natal'in BA (1996). Paleotectonics of Asia: fragments of a synthesis. In: Yin A, Harrison TM, editors. The Tectonic Evolution of Asia. Cambridge, UK: Cambridge University Press, pp. 486-640.

Shahbazi H, Siebel W, Pourmoafee M, Ghorbani M, Sepahi AA, Shang CK, Abedini MV (2010). Geochemistry and U–Pb zircon geochronology of the Alvand plutonic complex in Sanandaj–Sirjan Zone (Iran): new evidence for Jurassic magmatism. J Asian Earth Sci 39: 668-683.

Shaker Ardakani AR (2016). Post-collisional Plio-Pleistocene Anar-Dehaj adakitic subvolcanic domes in the central volcanic belt of Iran: geochemical characteristics and tectonic implications. Period Mineral 85: 185-200.

Shaker Ardakani AR, Arvin M, Oberhansli R, Mock B, Moeinzadeh SH (2009). Morphology and petrogenesis of pillow lavas from the Ganj ophiolitic complex, southeastern Kerman, Iran. J. Sci I R Iran 20: 139–151.

Shervais JW (1982). Ti-V plots and the petrogenesis of modern and ophiolitic lavas. Earth Planet Sci Lett 59: 101-118

Singh J, Johannse W (1996). Dehydration melting of tonalites: part II. Composition of melts and solids. Contri Mineral Petrol 125: 26-44.

Slovenec D, Lugovic B, Vlahovic I (2010). Geochemistry, petrology and tectonomagmatic significance of basaltic rocks from the ophiolite mélange at the NW external-internal Dinarides junction (Croatia). Geol Carpathica 61: 273-292.

Stocklin J (1968). Structural history and tectonics of Iran: a review. Am Assoc Petrol Geol Bull 52: 1229-1258.

Stolz AJ, Jochum KP, Spettel B, Hofmann AW (1996). Fluid- and melt-related enrichment in the subarc mantle: evidence from Nb/Ta variations in island-arc basalts. Geology 24: 587-590.

Sun S, McDonough WF (1989). Chemical and isotopic systematics of oceanic basalts: implications for mantle composition and processes. Geol Soc London Spec Publ 42: 313-345.

Tatsumi Y, Kosligo T, Nohda S (1995). Formation of a third volcanic chain in Kamchatka; generation of unusual subduction-related magmas. Contrib Mineral Petrol 120: 117-128.

Temizel I, Arslan M (2008). Petrology and geochemistry of Tertiary volcanic rocks from the İkizce (Ordu) area, NE Turkey: implications for the evolution of the eastern Pontide paleomagmatic arc. J Asian Earth Sci 31: 439-463.

Turner SP, Foden JD, Morrison RS (1992). Derivation of some A-type magmas by fractionation of basaltic magma: an example from the Padthaway Ridge, South Australia. Lithos 28: 151-179.

Thompson G (1991). Metamorphic and hydrothermal processes: basalt-sea water interactions. In: Floyd PA, editor. Ocean Basalts. Glasgow, UK: Blackie, pp. 143-73.

Wang T, Wang Z, Yana Z, Ma Z, He S, Fua C, Wang D (2016). Geochronological and geochemical evidence of amphibolite from the Hualong Group, northwest China: implication for the early Paleozoic accretionary tectonics of the Central Qilian belt. Lithos 248-251: 12-21.

Wilson M (1989). Igneous Petrogenesis: a Global Tectonic Approach. Boston, MA, USA: Unwin Hyman.

Winchester JA, Floyd PA (1976). Geochemical magma type discrimination: application to altered and metamorphosed basic igneous rocks. Earth Planet Sci Lett 28: 459-469.

Winchester JA, Floyd PA (1977). Geochemical discrimination of different magma series and their differentiation products using immobile elements. Chem Geol 20: 325-343.

Wood DA (1980). The application of a Th-Hf-Ta diagram to problems of tectonomagmatic classification and establishing the nature of crustal contamination of basaltic lavas of the British Tertiary volcanic province. Earth Planet Sci Lett 50: 11-30.

Woodhead J, Eggins S, Gamble J (1993). High-field strength and transition element systematics in island arc and back-arc basin basalts: evidence for multiphase melt extraction and a depleted mantle wedge. Earth Planet Sci Lett 114: 491-504.